Vibration Characteristics of the Fuel and Oxygen Turbopumps of the Space Shuttle's Main Engine

Technical Article

Summary. Some of the vibration characteristics of the SSME (space shuttle main engine) hydrogen and oxygen pumps are presented in this article. The space shuttle engine consists of three main rocket nozzles. Attached to each rocket engine are high-pressure fuel and oxygen pumps. Various vibration problems have been encountered with both pumps. Vibration spectra were analyzed by various techniques using synchronous tracking filters and FFT analyzers. The experimental data were correlated to theoretical predictions of resonance frequencies.

Edgar J. Gunter, Jr.
University of Virginia
Charlottesville, Virginia

The Rotor Dynamics Laboratory at the University of Virginia investigated for a period of four years various aspects of the dynamic and stability characteristics of the high-pressure hydrogen and oxygen pumps of the space shuttle's main engine (SSME). A schematic of the SSME is shown in Figure 1. This article presents some of the experimental techniques used in the investigation of vibration phenomena encountered with the pumps.

Theoretical Analysis of Hydrogen Turbopump

One of the two high-speed rotating pumps of the SSME engine supplies liquid hydrogen to the rocket nozzle; the hydrogen pump is labeled HPFTP (high-pressure fuel turbopump) in Figure 1. The other pump, labeled HPOTP, supplies oxygen. The liquid oxygen and hydrogen supplied to the rocket nozzle are fed into the combustion chamber of one of the three rocket engines of the space shuttle.

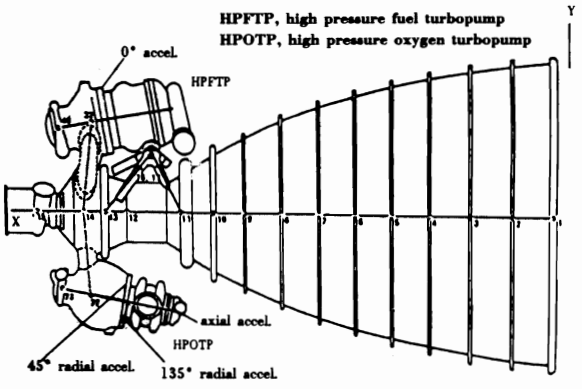

Figure 1. Schematic of the Space Shuttle Main Engine (SSME).

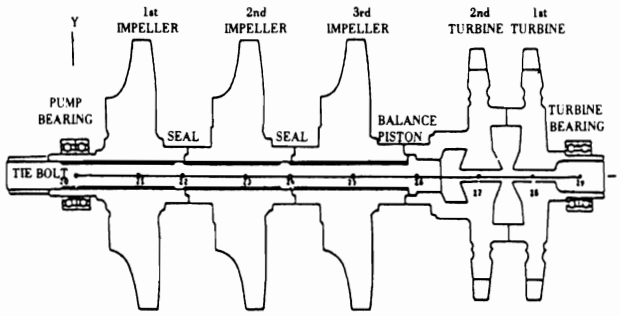

Figure 2. Cross Section of Hydrogen Pump.

A schematic diagram of the hydrogen pump is shown in Figure 2. The 125-pound pump, which was designed to operate at 37,500 RPM (625 Hz), has two turbine stages that drive three radial pump impellers. The two turbine stages were designed to develop up to 72,000 HP. The pump is therefore one of the highest energy density pumps ever built.

During the initial testing of the hydrogen pump a self-excited instability, which had been predicted by Childs [1], was observed at about 20,000 RPM (333 Hz). The operating speed of the pump was not able to exceed this value for a prolonged length of time without causing pump or bearing damage. In the original design of the hydrogen pump the rotor was supported by soft bearing mounts to lower the first two critical speeds below the operating range. The seals alone were sufficient to cause self-excited rotor whirl instability. It was predicted that a dramatic increase in the stability threshold speed of the pump could be obtained by stiffening the bearing supports and replacing the labyrinth seals with smooth,

straight seals [2, 3]. The instability problem was eliminated after these changes were incorporated into the hydrogen pump [4].

However, the stiffened bearing supports and new seals elevated the critical speeds. Analysis of early vibration data for the hydrogen pump (HPFTP) indicated that the bearing support stiffnesses were lower than the anticipated design values. These lower values meant that the second critical speed of the hydrogen pump was in the operating speed range. But, when spectra of early runs were analyzed, various resonance frequencies were found that had not been predicted by the original single spool critical speed analysis.

A more complex dynamic analysis was then undertaken that included the flexible pump casing and the hot gas manifold that attaches to the main engine. The combined axial, radial, and lateral rotor-casing modes could then be predicted. For example, Figure 3 represents the predicted critical speeds of the hydrogen pump corresponding to the in-plane direction. Depending on the values assumed for the balance piston and the bearing stiffnesses, it is possible to have several critical speeds in the operating speed range of the hydrogen pump [5].

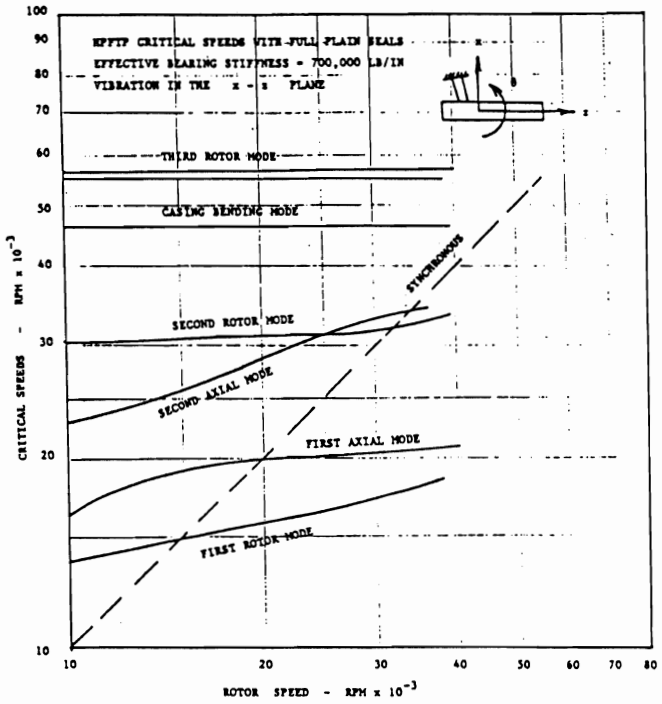

Figure 3. Critical Speed Plot of Hydrogen Pump.

Experimental Investigation of the Hydrogen Pump

Instrumentation available on the hydrogen pump consisted of various accelerometers on the pump casing and internal proximity probes to monitor relative shaft motion. Determination of a critical speed of the rotor required synchronous tracking on either the output of the proximity probe or the output of the accelerometers. Synchronous tracking necessitated a reference timing signal generated by shaft rotation. The reference timing signal and the vibration signal then had to be passed through a synchronous tracking filter to obtain amplitude and phase.

Two tracking filters were used: the Spectral Dynamics SD 119 Trim Balance Analyzer and the Bently Nevada Digital Vector Filter II. The Bently Nevada tracking filter can be used to record total, synchronous, or nonsynchronous motion as a function of shaft speed.

Unfortunately, the turbopump speed control signals are four pulses per shaft revolution instead of one pulse. Elaborate procedures had to be developed to produce a single pulse for the tracking filters. Figure 4 is a diagram of the instrumentation used to produce a single timing signal that would trigger the tracking filter.

Figure 4. Instrumentation Used in Data Reduction.

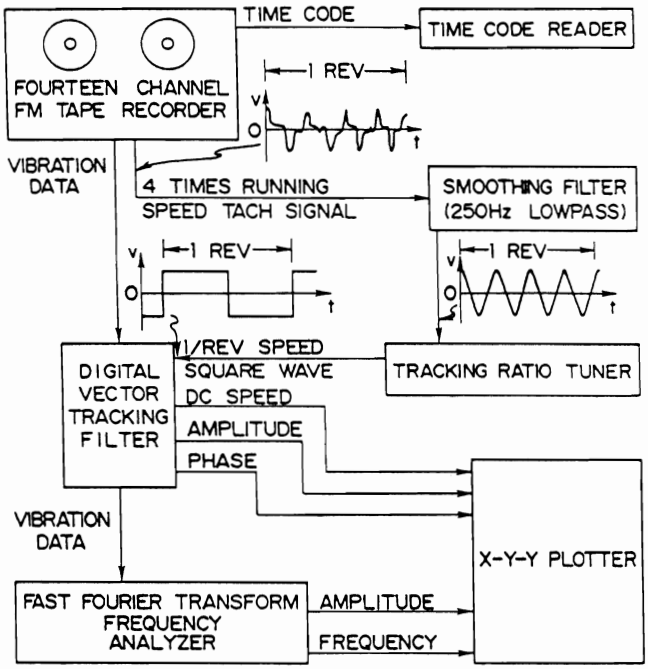

Data could be analyzed by one or a combination of three procedures: plotting total vibration amplitudes vs shaft speed of the pump, plotting the synchronous component of vibration and phase vs shaft speed, and analyzing the frequency spectrum of the vibration signal. The noise on the total vibration signal made the first type of plot almost useless. The vibration data were recorded on one-inch tape at 64 in./sec. and played back on a 14 channel FM tape recorder at reduced speed. A time code reader was used to monitor the times that data were recorded. The signal from the channel that picked up the four pulses per shaft revolution was first conditioned with a smoothing filter and then fed into the Spectral Dynamics Tracking Ratio Tuner Model SD 134A. This

procedure produced the required one square wave per revolution necessary to trigger the Bently Nevada Digital Vector Filter II. The digital vector filter produces DC output proportional to speed, amplitude, and phase.

The unfiltered (or total) amplitude of shaft motion of the hydrogen pump was plotted against running speed (Figure 5) during run up to rated power level (RPL). The considerable noise due to high-frequency components made it difficult to determine the critical speeds of the hydrogen pump. Figure 6, which contains only the synchronous component of the vibration shown in Figure 5, shows both run up and run down. It can be seen that the synchronous tracking filter has clarified the information contained in the vibration signals.

Figure 5. Shaft Motion of the Hydrogen Pump Plotted as a Function of Speed.

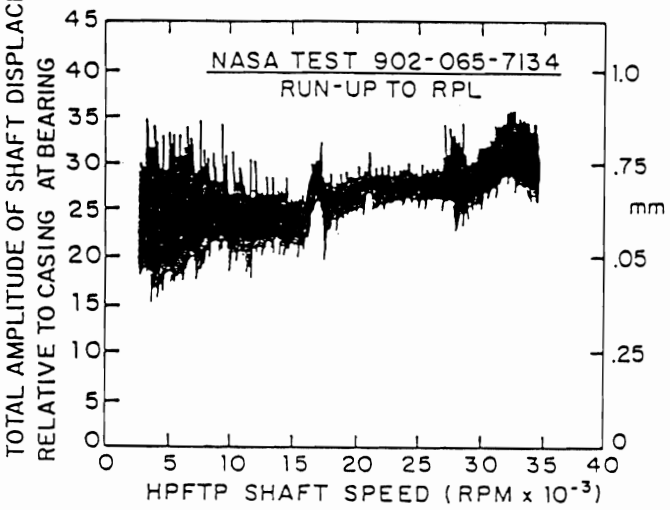

The peaks at 16,500 RPM (275 Hz) and 32,000 RPM (533 Hz) during run up represent the first and second critical speeds (Figure 6). These peaks did not appear during run down because of the rapid deceleration. When speed was held constant at 28,000 RPM (467 Hz) during run up, the vibration amplitude decreased considerably. This reduction also occurred at the RPL. It is possible that the drop in amplitude with time at constant rotational speed resulted from thermal changes in the system.

Figure 6. Synchronous Motion of Hydrogen Pump.

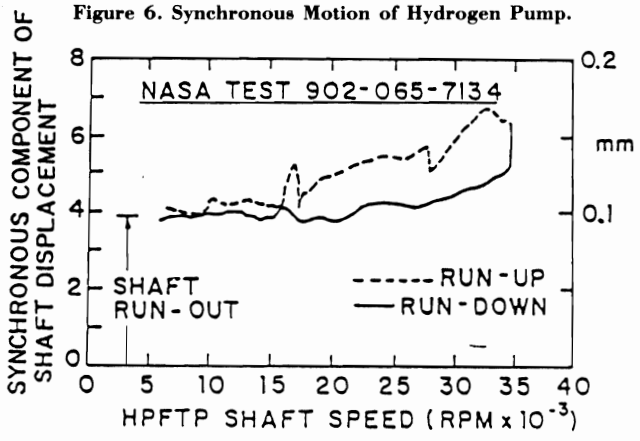

An estimate of bearing loading can be made from Figure 6. Shaft run out is approximately 4 mils. Peak amplitude at 32,000 RPM is 6.8 mils. Therefore, the relative motion at the second critical speed is approximately 2.8 mils. If effective bearing stiffness of the bearing support system is assumed to be 700,000 lb/in., a peak-to-peak load of 1,960 lbs. is indicated. This load is considerably in excess of the 400-pound design value for dynamic loading of the radial bearing. Because ball bearing life is inversely proportional to the cube of the bearing load, the life of the bearings could be reduced by a factor of more than 100 from the design value. For example, sustained operation under such conditions could reduce bearing life from 50 hours to only 30 minutes.

After bearing changes had been made in the pump, the proximity probe was not available for later investigations of shaft motion. Accelerometer measurements had to be used to determine resonance frequencies of the system. The following instruments were used to evaluate spectral characteristics of both the oxygen and hydrogen pumps: Spectral Dynamics SD360 Digital Signal Processor, Hewlett Packard 5420A Digital Signal Analyzer, HP 9845B Computer, and HP 9872A Digital Plotter.

Figure 7 is the time history waveform of the 0° radial accelerometer for the hydrogen pump operating at 100% RPL. The amplitude of motion is about ± 30 g's. One cycle of running speed is shown. Very high-frequency components apparent in the accelerometer signal mask the structural modes of the rotor and casing close to the operating speed. The same signal was passed through a low-pass filter (Figure 8) so that the frequency spectrum close to operating speed could be examined.

Figure 9 shows the peak channel-hold for the 90° casing accelerometer (located normal to the plane of the

Figure 7. Unfiltered Waveform of the 0° Radial Accelerometer of the Hydrogen Pump at 100% Rated Power Level (RPL).

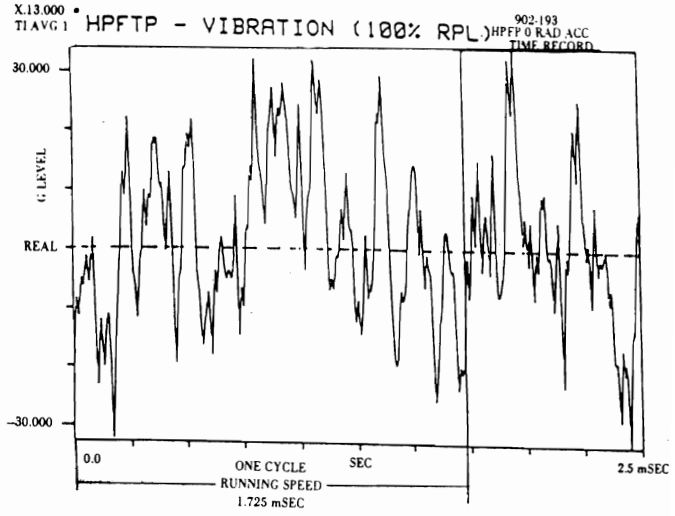

hydrogen pump and nozzle) for the hydrogen pump; the higher frequencies have been filtered from the signal. The channel-hold procedure was used to capture the maximum spectrum produced by the pump. The engine was allowed to coast down from 109% RPL to zero speed. A resonant frequency was apparent in the system at 35,460 RPM (591 Hz), which is the design operating speed of the pump.

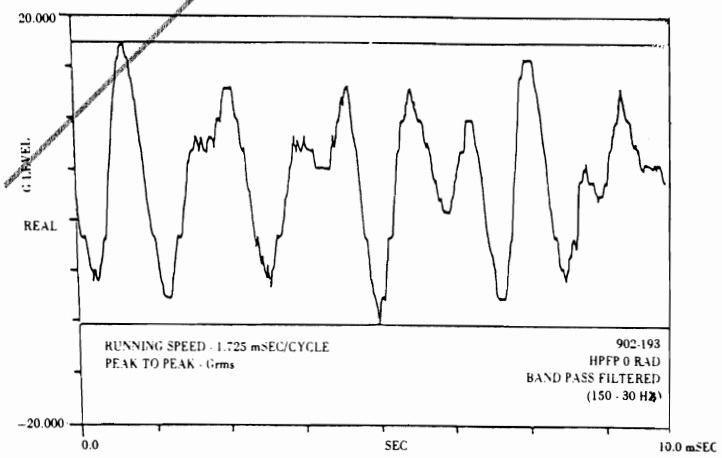

Figure 8. Filtered Waveform of the 0° Radial Accelerometer of the Hydrogen Pump at 100% RPL.

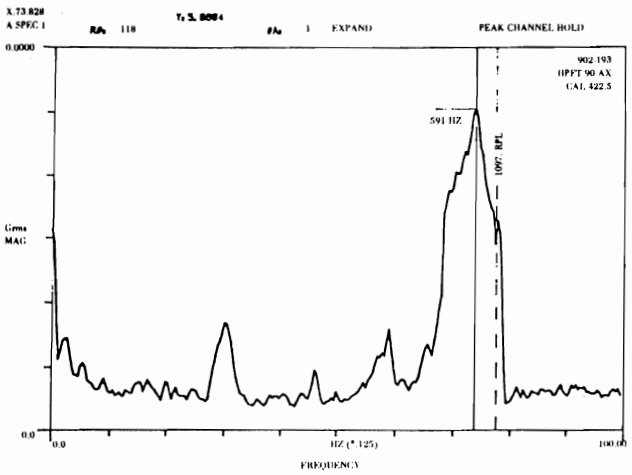

Figure 9. Peak-Channel Hold of 90° Axial Accelerometer of Hydrogen Pump from 109% RPL to 0% RPL.

Theoretical Analysis of Oxygen Turbopump

The oxygen pump, labeled HPOTP (high-pressure oxygen turbopump), is shown in Figure 1. This pump was designed to supply liquid oxygen (LOX) at 1,153 lbs/sec. to the engine. Supply pressure to the main pump is 4,974 psi; supply pressure to the small preburner pump is 8,070 psi.

The rotor of the oxygen pump shown in Figure 10 is supported by two 45 mm ball bearings at the pump end (left) and by two 55 mm ball bearings at the turbine

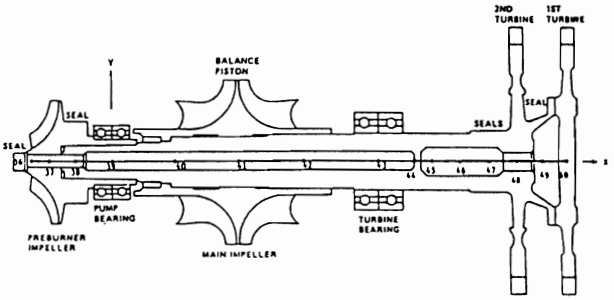

Figure 10. Oxygen Pump.

end (right). The two-stage hot-gas turbine that drives the oxygen pump is shown at the right. The main pump, which is represented by the central impeller, has a dual-flow configuration. The oxygen pump was designed to operate from 22,000 RPM (367 Hz) to 28,000 RPM (467 Hz) and is to be free of critical speeds in this range according to original NASA specifications. The design time for operation of the oxygen pump during full power level (FPL) is 730 seconds.

Figure 11 represents experimental data obtained during a test run. Synchronous motion of a radial oxygen pump casing accelerometer located at the casing center plane split line was plotted vs shaft speed for run up and run down. During run up two major resonant peaks are obtained at about 22,000 RPM and 27,000 RPM (450 Hz). A predominant peak occurred at 26,000 RPM (433 Hz) during run down.

Figure 11. Synchronous Output of Radial Accelerometer of Oxygen Pump as a Function of Speed.

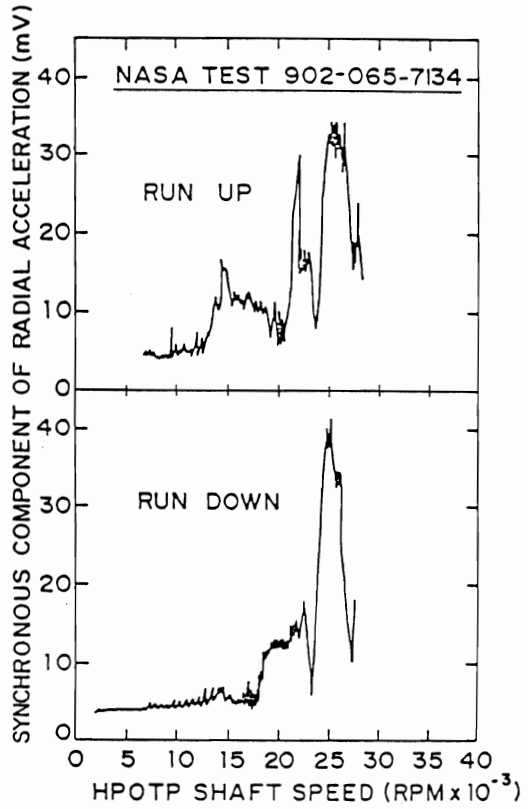

According to the original design specifications there should not be any critical speeds in the operating speed range. However, later tests of the oxygen pump conducted in a balancing facility showed two critical speeds in the operating speed range. The total bearing stiffness of the 45 mm bearings may be only on the order of 400,000 lb./in. instead of the originally predicted value of 700,000 lb./in.

The predicted mode shape for the oxygen pump with the reduced preburner bearing mode stiffness is shown in Figure 12. The second critical speed is predicted to be 25,350 RPM (423 Hz). Note that the overhung turbine has little motion at the second critical speed, which is a node point. Turbine balancing therefore has no effect on the second critical speed of the oxygen pump.

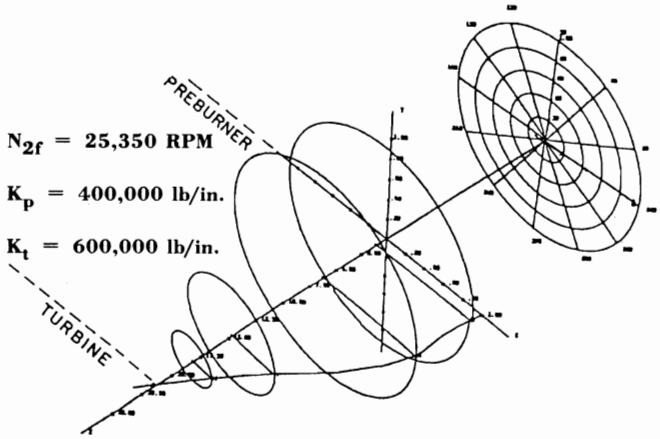

Figure 12. Undamped Second Forward Critical Speed of Oxygen Pump at 27,000 RPM.

Experimental Investigation of the Oxygen Pump

The procedures used to investigate the oxygen pump were similar to those used for the hydrogen pump. However, because the speed of the hydrogen pump had often been detected by accelerometers mounted on the casing of the oxygen pump, it was decided to evaluate the influence of this excitation on the oxygen pump. Such an evaluation required superposition of an accurate speed signal from the hydrogen pump on taped vibration data from the oxygen pump. The vibration at the oxygen pump was tracked as a function of hydrogen-pump speed by dubbing this speed on the tape and synchronizing the recording with two time code readers.

In Figure 13 the synchronous motion of the accelerometer on the casing of the oxygen pump has been tracked as a function of shaft speed of the hydrogen pump. The hydrogen pump operates at a slightly higher speed and acts as a vibration excitor of the oxygen pump. Data from the tracking filter, which is synchronous with the speed of the hydrogen pump, indicated resonant frequencies within the operating speed range of both pumps.

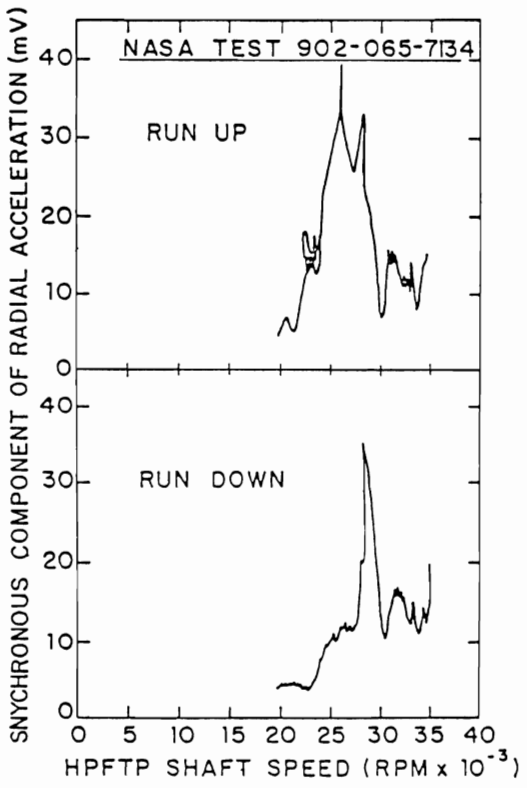

Figure 13. Vibration from 45° Radial Accelerometer of Oxygen Pump as a Function of Hydrogen Pump Speed.

During run up, a resonant frequency occurred at about 25,000 RPM (417 Hz) that corresponded to vibration data obtained during run up and run down of the hydrogen pump (Figure 13). Another resonant frequency that occurred at about 28,000 RPM (467 Hz) during run up was also the predominant frequency during run down. The data plotted in Figure 13 thus indicate three resonant frequencies in the operating speed range – at 22,000 RPM (367 Hz), 26,000 RPM (433 Hz), and 28,000 RPM. The 540° phase shift observed also indicates passage through three resonant frequencies [4].

A cascade plot for the axial 90° accelerometer on the preburner is given in Figure 14 for speeds from 60% RPL to 100% RPL. The low-level motion of the oxygen pump, shown as a dotted line labeled O_2 whirl, may possibly be associated with a self-excited whirl motion of the oxygen pump at the first critical speed.

The vibration responses due to synchronous excitation of the oxygen pump and nonsynchronous excitation of the hydrogen pump are also shown. The resonant frequency of the oxygen pump at 27,960 RPM (466 Hz) corresponds to 100% RPL. The amplitude increase on the oxygen pump at 23,680 RPM (378 Hz) may indicate another critical speed. Peaks occurred on the hydrogen pump at 28,080 RPM (468 Hz), 30,840 RPM (514 Hz), and 35,220 RPM (587 Hz). The fact that 35,220 RPM (587 Hz) is the operating speed of the pump indi-

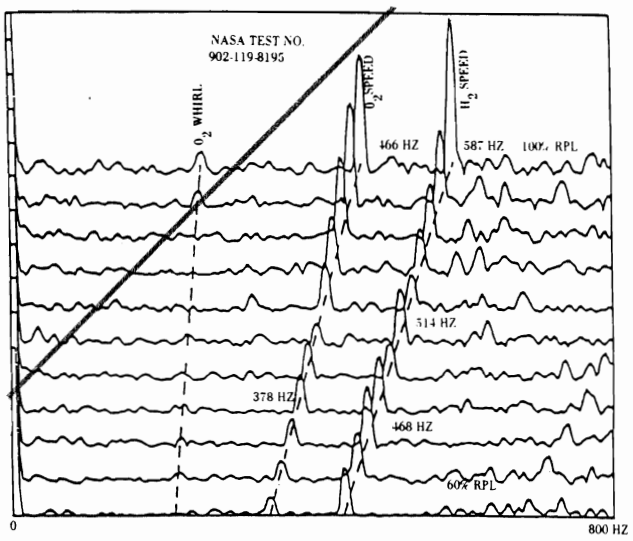

Figure 14. Cascade Diagram of 90° Axial Accelerometer of Oxygen Pump.

cates that the hydrogen pump may also have been operating on a resonant frequency. In addition, the vibration of the oxygen pump peaks at 28,080 RPM (468 Hz), indicating a possible resonant frequency of the oxygen pump at the operating speed of the hydrogen pump.

The oxygen pump malfunctioned several times during the experimental testing of the SSME. The data recorded in one early incident are shown in Figure 15. The engine was programmed to operate at 90% RPL for 31 seconds, increase to 100% RPL, and return to 90% for the remainder of the run. Raw data passed through a 250 Hz to 500 Hz filter showed that amplitudes were increasing rapidly on the radial accelerometer of the

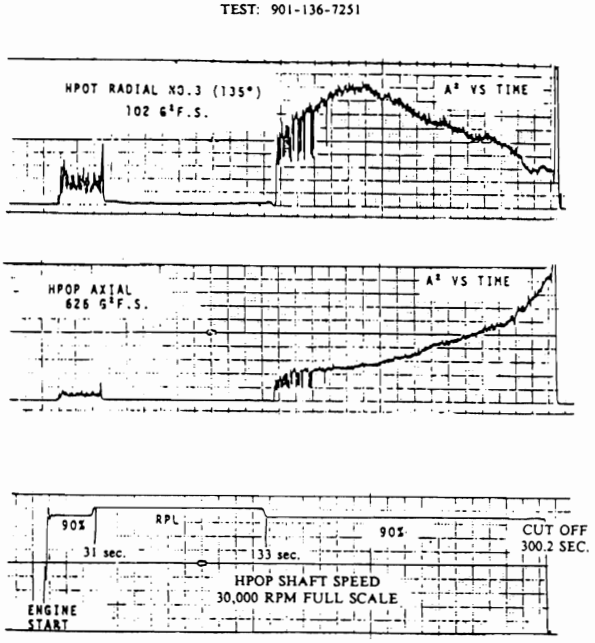

Figure 15. Total Motion of Radial and Axial Accelerometers of Oxygen Pump during Failure Run.

preburner pump (PB) and the axial accelerometer of the oxygen pump. The output of the radial accelerometer at the turbine end of the oxygen pump (HPOT) actually decreased after 180 seconds; the outputs of the radial accelerometers at 45° and 135° of the preburner pump and the axial accelerometer (HPOP) increased rapidly. At the time of failure, therefore, the casing had a cantilever mode of motion in which there were both radial and axial displacements. Such data do not provide much insight as to the frequencies at which critical speeds or resonant modes are occurring, however.

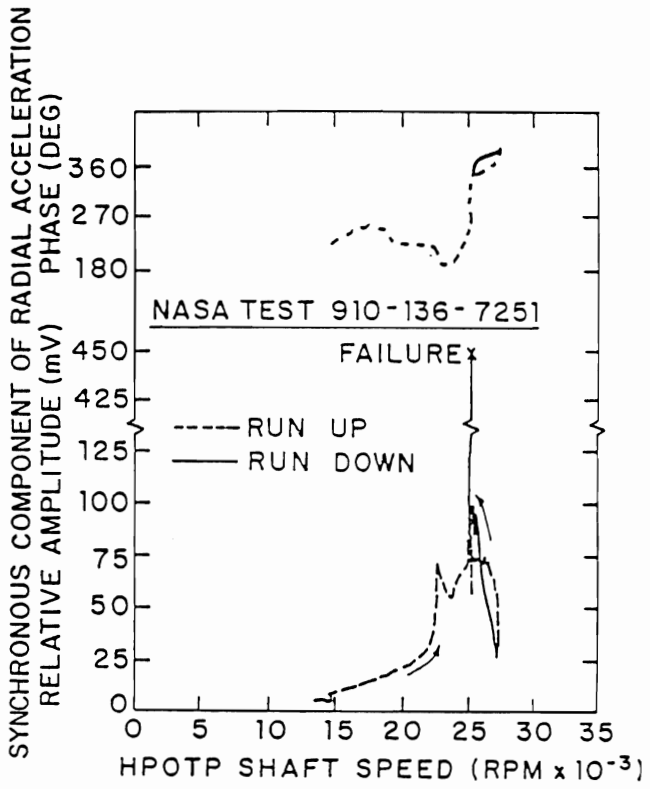

Figure 16. Synchronous Component of #3 Radial Accelerometer of Oxygen Pump as a Function of Speed.

Synchronous tracking was used to plot the synchronous radial acceleration of the oxygen pump as a function of its shaft speed as shown in Figure 16. The rotor passed through two resonances at 22,000 RPM (367 Hz) and 25,500 RPM (425 Hz) during run up. The resonance at 25,500 RPM, which appeared to dominate, corresponds to operation at 90% RPL. After 100% RPL was attained the speed was reduced, and the rotor was operated at 90% RPL. Rotor amplitude increased at this speed until failure occurred. The dotted line in the upper half of Figure 16 represents the change in phase angle as the rotor passed through 25,500 RPM. The 180° phase shift corresponds to passage through a resonant frequency.

The peak-channel hold spectrum of the 45° radial accelerometer of the oxygen pump during deceleration from 109% RPL to 90% RPL is shown in Figure 17.

Note the pronounced resonant frequency at 27,780 RPM (463 Hz). The magnitude of the peak amplitude is 10 g_{rms}. Results from the other accelerometers on the oxygen pump were similar. The data indicated that the oxygen pump has a major resonant frequency between 27,000 RPM (450 Hz) and 28,200 RPM (470 Hz) that could represent the second critical speed of the oxygen pump. The mode may be particularly sensitive to excitation because a nozzle bending mode was also predicted in this range.

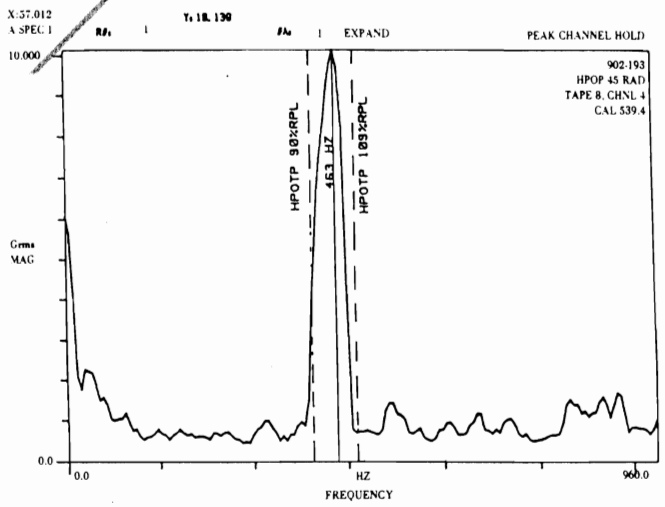

Figure 17. Engine Deceleration from 109% RPL to 90% RPL of 45° Radial Accelerometer of Oxygen Pump.

Conclusions

Accelerometers and other instrumentation were placed on the high pressure hydrogen and oxygen pumps of the space shuttle main engine after excessive vibrations had been observed. This article has presented various procedures by which the data were analyzed. Two basic types of instrumentation used in the data reduction were synchronous tracking filters and fast Fourier transform signal analyzers. The synchronous tracking filters were used to observe pump and casing resonance frequencies as functions of the speeds of the pumps. The procedure facilitated the identification of pump frequencies and structural resonance frequencies in the operating speed range. The synchronous tracking procedure required a properly conditioned reference signal for pump speed. Adequate speed signals were not always available for use in certain test runs of the SSME. The incorporation of once-per-revolution timing indicators in both the hydrogen and oxygen pumps is highly recommended. The timing indicators allow proper observation of the critical speeds of the pumps and of absolute phase-angle changes.

FFT analyzers were used exclusively in cases in which synchronous tracking could not be performed. They allowed observation of frequencies over various band widths and generation of cascade plots of vibration spectra at different power levels. Various frequencies were detected by an accelerometer with this procedure. Thus, tracking filters and FFT analyzers can be used to obtain an understanding of the resonant frequencies and mode shapes of a vibrating structure if a proper timing reference signal is incorporated to monitor pump speeds. Correct interpretation of the data can lead to recommendations for corrective measures for reducing vibrations for both hydrogen and oxygen pumps.

References

1. Childs, D.W., *The SSME High Pressure Fuel Turbopump Rotordynamic Instability Problem,* J. Engrg. Power, Trans. ASME, Paper No. 77-GT-49 (Dec. 1976).

2. Allaire, P.E., Gunter, E.J., Lee, C.P., and Barrett, L.E., *Final Report—The Dynamic Analysis of the Space Shuttle Main Engine-High Pressure Fuel Turbopump; Part II: Load Capacity and Hybrid Coefficients for Turbulent Interstage Seal,* Report No. UVA/528140/ME76/103, University of Virginia, Charlottesville (Sept. 1976).

3. Gunter, E.J., Barrett, L.E., Palazzolo, A.B., and Allaire, P.E., *Final Report—The Dynamic Analysis of the Space Shuttle Main Engine-High Pressure Fuel Turbopump; Part II: Linearized Stability Analysis,* Report No. UVA/528140/ME76/104, University of Virginia, Charlottesville (Sept. 1976).

4. Eck, M.C., *Solution of the Subsynchronous Whirl Problem in the High Pressure Hydrogen Turbomachinery,* Paper No. 78-1002, Amer. Inst. Aeronaut. Astronaut, 14th Joint Propulsion Conf., Las Vegas, NV (July 25-27, 1978).

5. Gunter, E.J., Li, D.F., Allaire, P.E., and Barrett, L.E., *The Dynamic Analysis of the Space Shuttle Main Engine—High Pressure Fuel Turbopump; Part I: Critical Speed Analysis,* Report No. UVA/528140/ME76/102, University of Virginia, Charlottesville (Sept. 1976).

Acknowledgements

The author would like to acknowledge Professor Ronald D. Flack, Lyle A. Branagan, John D. Heinzmann, and Alan B. Palazzolo for their extensive and time-consuming efforts in the data reduction. Acknowledgement is also given to Bently Nevada Corporation for furnishing the digital vector filters used in the data reduction. This work was supported in part by NASA contract NAS8-31951-15.